

Controlling nickel silicide phase formation by Si implantation damage

M. Guihard^a, P. Turcotte-Tremblay^a, S. Gaudet^b, C. Coia^b, S. Roorda^a, P. Desjardins^b,
C. Lavoie^c, F. Schiettekatte^{a,*}

^aDépartement de Physique, Université de Montréal, Montréal, Canada

^bDépartement de Génie Physique, École Polytechnique de Montréal, Montréal, Canada

^cIBM T.J. Watson Research Center, Yorktown Heights, New York, USA

ARTICLE INFO

Article history:

Available online 8 February 2009

PACS:

66.30.-h

68.55.-a

64.60.-i

Keywords:

Nickel monosilicide

NiSi

Ion implantation

ABSTRACT

In the context of fabrication process of contacts in CMOS integrated circuits, we studied the effect of implantation-induced damage on the Ni silicide phase formation sequence. The device layers of Silicon-on-insulator samples were implanted with 30 or 60 keV Si ions at several fluences up to amorphization. Next, 10 or 30 nm Ni layers were deposited. The monitoring of annealing treatments was achieved with time-resolved X-ray diffraction (XRD) technique. Rutherford Backscattering Spectrometry and pole figure XRD were also used to characterize some intermediate phase formations. We show the existence of an implantation threshold (1 ions/nm²) from where the silicidation behaviour changes significantly, the formation temperature of the disilicide namely shifting abruptly from 800 to 450 °C. It is also found that the monosilicide formation onset temperature for the thinner Ni deposits increases linearly by about 30 °C with the amount of damage.

© 2009 Elsevier B.V. All rights reserved.

1. Introduction

Nickel monosilicide (NiSi) is the current material of choice for metal to semi-conductor contacts in CMOS devices. It is synthesized by solid-state reactions induced by annealing thin Ni layers deposited on Si substrates. Compared to CoSi₂ which it replaces, NiSi also presents some advantages among which we find a lower resistivity, a reduced Si consumption and a lower formation temperature. Even though the Ni–Si system has been thoroughly studied for the last 40 years [1], the current industry needs in terms of reduced device dimensions require a better understanding of the microstructure and reaction pathways prevailing in small silicided circuit structures. The Ni–Si system is complex with six phases stable at room temperature (RT): the metal-rich phases as Ni₃Si, Ni₃₁Si₁₂, Ni₂Si and Ni₃Si₂, the monosilicide (NiSi) and the disilicide (NiSi₂). NiSi thin film reactions are commonly reported to result in the successive formation of Ni₂Si, NiSi and NiSi₂ layers [2], the monosilicide forming only once the Ni is completely exhausted. Although NiSi₂ is the final phase in the sequence of all excess-Si reactions, being in equilibrium with the latter, the monosilicide is the low-resistivity phase which bears a technological interest.

NiSi thin films tend to either agglomerates or turns into disilicide [3], reducing their applicability to microelectronics. To stabi-

lize these films, a common practise in the industry is to introduce alloying elements like Pt into the metal layer before the reaction [4,5]. Another interesting solution is to modify the structure of the underlying substrate by ion implantation. The extra free energy stored in implantation-induced damages and released during annealing [6], can be used to promote the silicidation, and potentially reduce the thermal budget required for complete conversion of the Ni to NiSi layers. It has been shown that preamorphization of Si substrate leads to a considerably reduced growth temperature of the disilicide phase which then forms by a diffusion-controlled process [7].

In this paper, we investigate the effect of partial damage induced by Si implantation in the substrate on the kinetics of Ni–Si thin film reactions. It is shown that the temperature onset for the NiSi growth increases linearly with fluence, in opposition to the desired effect, and that a threshold fluence exists, associated to the amorphization threshold, above which the NiSi₂ growth is advanced.

2. Experiments

SOI wafers with a (001) Si device layer of 115 ± 15 nm and an oxide layer of 150 ± 30 nm were implanted with 30 keV ²⁸Si⁻ ions using a 1.7 MV Tandemron operated in accel–decel mode, and with 60 keV ²⁸Si⁻ using a 100 kV ion implanter, both equipped with a negative ion sputtering source. Implantation fluences ranged from 1 × 10¹³ to 3 × 10¹⁵ ions/cm² on a sample holder cooled with li-

* Corresponding author.

E-mail address: francois.schiettekatte@umontreal.ca (F. Schiettekatte).

quid nitrogen and surrounded by a negatively biased Faraday cage. In order to avoid channeling in the crystalline substrate the normal of the sample was tilted by 7° off the ion beam axis. Current measurements on the target were frequently compared to the readings of a Faraday cup. The conversion factor to express the displacement per atom (dpa) in fluence (ions/cm²) is 6.7×10^{14} with 30 keV ²⁸Si⁺ ions. Rutherford Backscattering Spectrometry (RBS) measurements in channeling mode were carried out on each sample using a 2 MeV ⁴He⁺ beam to assess the damage profiles.

Ni films with thicknesses of 10 or 30 nm were deposited by magnetron sputtering on the implanted samples. All the substrates were etched in a 1% HF solution prior to deposition. All samples with the same Ni thickness were deposited together in a single run.

X-ray diffraction measurements were carried out at the National Synchrotron Light Source (NSLS) (Brookhaven National Laboratory). In these experiments, ramp-type annealings were performed from 100 to 900 °C at 3 °C/s. The phase formation process was monitored by time-resolved X-ray diffraction at a wavelength of 1.797 Å. Further details of this experiment are given elsewhere [8,9]. The detector consists of a linear CCD camera covering a range of 14° in 2θ . In order to cover the 2θ range between 22° and 62° , three identical ramp-anneals were acquired for each implantation fluence, with the detector centered at 29° , 42° and 55° . The samples were tilted so their surface normal was off by around 2° from the X-ray incidence plane in order to avoid intense peaks from the c-Si substrate. The temperature scale was calibrated using the Si–Au, Si–Al and Si–Ag eutectic melting points, to better than $\pm 3^\circ$ C. Ramp anneals were carried out under an atmosphere consisting of 99.999% pure He further purified using Ti metal at high temperature. A four point probe measurement was also performed for each ramp, providing the sheet resistance during the process.

Initial ramp-anneals were used to determine critical stages of the reaction at which we interrupted subsequent annealing experiments. Following these quenches, XRD was carried out at RT on a separate beam line where diffraction pole figures were acquired in order to perform the phase identification and determine thin film texture. For these measurements, the wavelength was set to 1.0507 Å and an area detector was used. Details of the method are described elsewhere [10]. Complementary RBS measurements were also performed at either normal or grazing (70°) incidences to assess the layer composition.

3. Results and discussion

Fig. 1 shows RBS profiles obtained in channeling mode for 30 keV ²⁸Si⁺ implantation at different fluences. Curves taken at random incidence on c-Si substrate or on the fully amorphous region are shown as reference. Compared to the undamaged crystalline part of the sample, the fully amorphized region appears thinner by ~ 3 nm, a result we ascribe to sputtering during implantation. An increase in the substrate's surface roughness is hence expected, perhaps with some effect on the phase formation. For a damage dose of 0.015 dpa (1×10^{13} Si/cm²), the top Si layer is still mostly crystalline. As the damage increases with the ion dose, we reach partial amorphization with some c-Si regions remaining at the surface. Full amorphization is achieved at 4.5 dpa (3×10^{15} Si/cm²). The depth of the damaged region, approximately 60 nm, indicates that there is enough amorphized Si to fully convert 10 nm Ni layers to NiSi₂ (10 nm of Ni will consume 36.6 nm of Si to produce 36.1 nm of NiSi₂). On the other hand, there is not enough damaged Si to achieve full conversion of 30 nm of Ni which would require 109.8 nm of Si. In order to impart damage to the entire Si layer, a 60 keV energy beam is needed, which causes the interface with the buried oxide layer of the SOI substrate to be damaged as well.

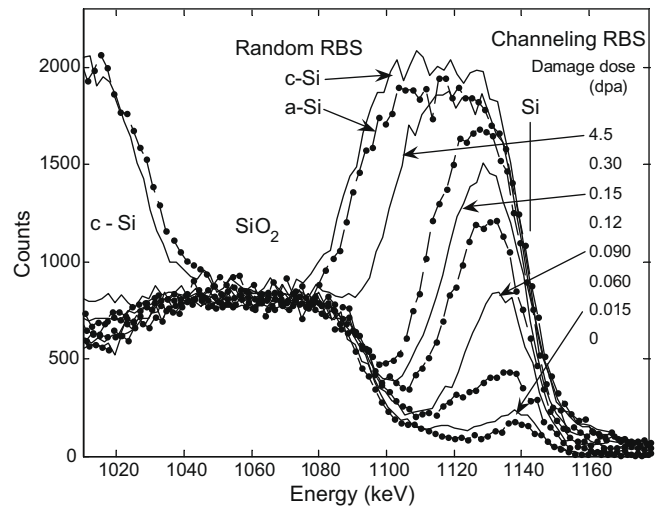


Fig. 1. RBS-channeling spectra along the $\langle 100 \rangle$ axis of SOI samples for which the top layer has been implanted with 30 keV ²⁸Si⁺ ions at fluences ranging from 1×10^{13} to 3×10^{15} ions/cm². The two top curves were taken at random incidence (7° off normal) on c-Si substrate and on sample with maximum damage.

Fig. 2 shows two sets of time-resolved XRD measurements acquired during ramp-anneals of 10 nm Ni layers deposited on unimplanted (a–c) and implanted (d–f) SOI substrates. The latter were implanted to the maximum damage dose of 4.5 dpa. The three figures presented for each implantation condition correspond to detector center positions of 29° , 42° and 55° in 2θ . The phase identification proposed was performed using the Joint Committee on Powder Diffraction Standard Database (JCPDS datasheets 04–0850, 73–2092, 38–0844, 80–0018) and supported by the analysis of the pole figure measurements.

Fig. 2(a)–(c) presents the typical phase formation sequence for the Ni–Si system with 10 nm of Ni. At about 200 °C, Ni starts to react resulting in the growth of the Ni₂Si phase evidenced by the (301)/(121) and (002) reflections of its orthorhombic crystal structure around 54° and 57.5° , respectively. Next, centered at 56.5° and around 330 °C, is an intense peak which is still under investigation and corresponds well to the hexagonal θ -Ni₂Si phase [11]. This phase apparently grows at the expense of the previous orthorhombic Ni₂Si. But as the temperature increases, the latter reappears as the hexagonal phase disappears. The orthorhombic NiSi phase simultaneously appears and is revealed by the following diffraction peaks: (101) in Fig. 2(a), (011)/(002) and (102)/(111) in Fig. 2(b), and (112), (211)/(202), (103) in Fig. 2(c). The shift towards lower diffraction angles observed for most of these NiSi peaks is associated to the thermal expansion of the materials, which results in increasing d-spacings with increasing temperature. The trend is however reversed for the NiSi(011) and (111) peaks in Fig. 2(b) as a consequence of a negative thermal expansion coefficient of the b axis of the orthorhombic structure [12]. Only few noticeable changes could be observed in the reaction for implantation fluences ranging from 1×10^{13} to 1×10^{14} Si/cm², as detailed below.

For fluences above 2×10^{14} Si/cm² the behaviour is similar to the one shown in Fig. 2(d)–(f), which present the reaction of a 10 nm Ni layer with a Si substrate implanted to a damage dose of 4.5 dpa (3.0×10^{15} Si/cm²). Additional samples were quenched at 269, 350, 465 and 575 °C (vertical lines in Fig. 2(d)–(f)) for further phase identification using pole figure XRD analysis as well as RBS at grazing incidence (70°). In the later technique, layer compositions were given as a function of depth by comparing the data with SIMNRA/RESOLNRA simulation [13], the depth resolutions being around 7 nm for Ni and 14 nm for Si. In addition to this weak

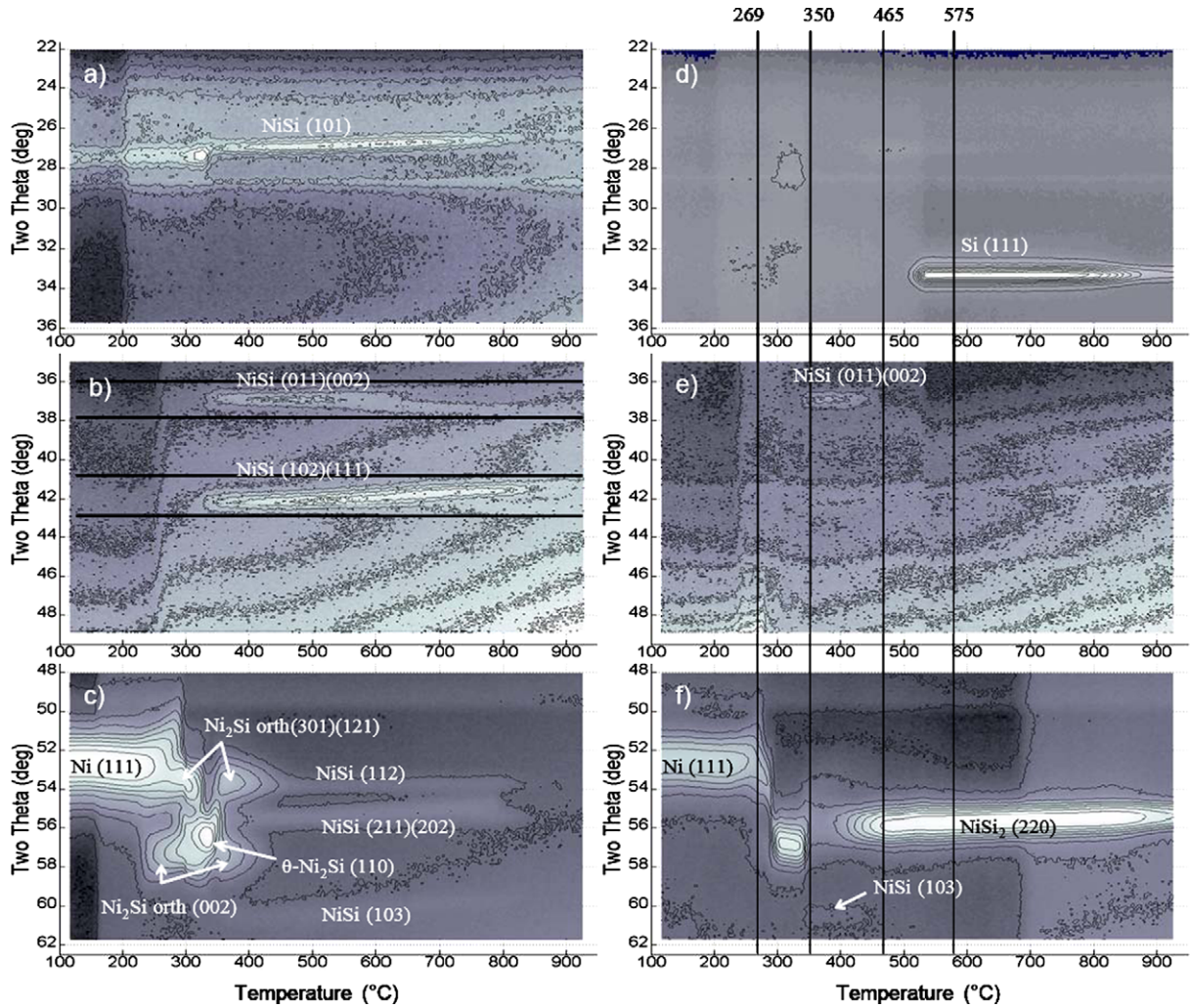


Fig. 2. Time-resolved XRD of 10 nm Ni deposited on SOI during ramp-anneals at 3 °C/s for three different angle ranges. Left column: unimplanted samples; right column: samples implanted with 30 keV $^{28}\text{Si}^-$ at a damage dose of 4.5 dpa (3.0×10^{15} ions/cm 2). Vertical lines: temperatures at which samples were quenched for further pole figure and RBS measurements. Horizontal lines in (b): angular range of peak integration.

resolution, possible co-existence of different phases in the Ni–Si system [14] could complicate the simulation. In spite of that, relatively precise layer thicknesses could be deduced and several observations can be made.

First, in Fig. 2(f), the sequence of the metal-rich phase formation between 200 and 400 °C is drastically different. Although the Ni(111) peak is always present, the orthorhombic Ni $_2$ Si(301)/(121) and (002) peaks originally observed around 200 and 320 °C are not present in this measurement geometry. However, the sample quenched at 269 °C reveals a Ni layer 1 ± 0.5 nm thick on 12.5 ± 0.5 nm of Ni $_2$ Si, as simulated by RBS (see Fig. 3). Second, the evolution of the NiSi peaks has changed (see Fig. 2(e)). Only a low intensity NiSi (011)/(002) peak remains at 37° over a significantly reduced temperature range. It vanishes by 450 °C instead of 850 °C in the low damage dose regime. The presence of NiSi is supported with the sample quenched at 350 °C. A good SIMNRA simulation fit is obtained considering a 19.9 ± 0.5 nm layer of NiSi on 90 ± 1 nm of Si and pole figures strongly suggest NiSi even if the growth texture is still under investigation. Finally, two intense peaks, which could be attributed either to the NiSi $_2$ phase or poly crystalline Si (poly-Si), are visible around 56° and 33.5° and appear at 400 and 520 °C respectively (Fig. 2(d) and (f)). At 465 °C, RBS simulation fits the experimental spectrum considering 1.8 ± 0.5 nm of NiSi on 29.8 ± 0.5 nm of NiSi $_2$ on 81 ± 1 nm of Si

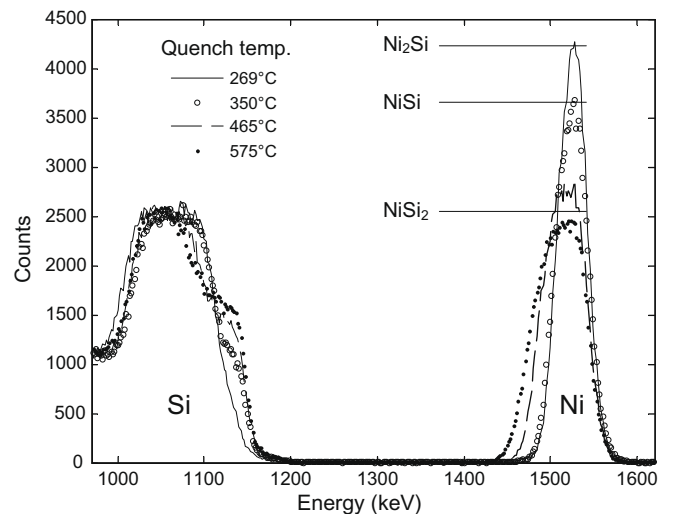


Fig. 3. RBS spectra of 10 nm samples, implanted with 30 keV Si ions at fluence of 1×10^{15} /cm 2 , and annealed at 3 °C/s up to 269, 350, 465 and 575 °C. Horizontal solid lines represent the expected Ni signal for Ni $_2$ Si, NiSi and NiSi $_2$. A 2 MeV $^4\text{He}^+$ ion beam at 70° incidence was used.

and the presence of both monosilicide and disilicide is supported by pole figure data. At 575 °C, the best RBS simulation is obtained with Ni_{0.3}Si_{0.7} (39 ± 1 nm) on Si (71 ± 1 nm) while the pole figures suggest the presence of crystalline NiSi₂ and poly-Si with, respectively, (220) and (111) planes parallel to the sample surface. Hence, combined XRD and RBS characterization strongly suggests that the peak around 56° can be attributed to the NiSi₂ phase while the peak at 33.5° can be attributed to a poly-Si phase, which has probably recrystallized from the NiSi₂/a-Si interface. The stoichiometry obtained by RBS, slightly different from the disilicide one, could result from layer roughness or lateral co-existence of both NiSi₂ and c-Si grains.

3.1. Influence of implantation

In Fig. 4, we show the onset temperature of the NiSi formation and the beginning of its disappearance as a function of the damage dose for 10 nm Ni (triangles) and 30 nm Ni (circles). The temperatures were determined by locating the slope change in the diffracted intensity summed over a range of 2° 2θ centered on the peaks of interest (see horizontal lines in Fig. 2(b)). The onset temperature of the monosilicide formation was determined to ±3 °C while the uncertainty is estimated to ±10 °C for the NiSi peak decrease. Two points deserve special attention from the 10 nm data; one at 0.09 dpa (6 × 10¹³ Si/cm²) and the other one at 0.75 dpa (5 × 10¹⁴ Si/cm²). They both displayed an unexpectedly large temperature delay in the formation of the metal-rich phases, and the orthorhombic Ni₂Si phase seemed absent from the reaction stage preceding the formation of the hexagonal Ni₂Si phase. We believe this retarded reaction could be the result of an insufficient HF cleaning. These samples were not included in subsequent curve fitting.

From Fig. 4(a), we observe that the NiSi onset temperature for the 30 nm case undergoes an abrupt increase. The onset suddenly shifts from about 335 °C to about 370 °C in the damage dose inter-

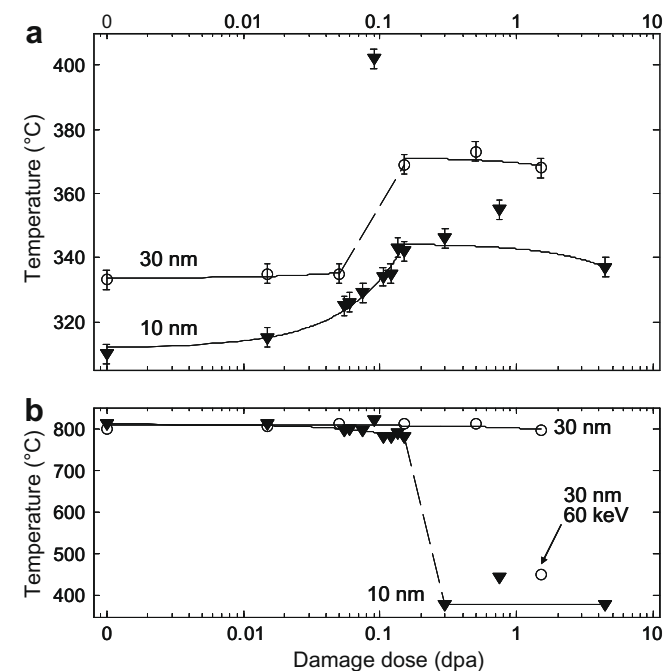


Fig. 4. Semi-log plots of the onset temperature in (a) and of the disappearance temperature in (b) of the NiSi phase, both as a function of the implantation damage dose. Circles and triangles are respectively for 30 nm and 10 nm of Ni deposited. The uncertainty in (b) is of the size of the symbols. Solid lines are linear fits while dashed lines are guides to the eye.

val between 0.05 and 0.15 dpa (3 × 10¹³ and 1 × 10¹⁴ ions/cm²). Both regimes are represented by solid lines which are linear fits. The dashed line is only there to emphasize the 35 °C step between them. We thus clearly see a threshold in the implantation damage above which the silicidation behaviour changes significantly. This change arises for damage doses at which the superlinear damage accumulation regime due to a-Si cluster formation is usually observed [15,16]. In the case of 10 nm Ni, we first note that at any damage dose, the NiSi formation starts 20–30 °C below that of 30 nm Ni samples. Next, the change between low and high damage doses is smoother. Between 0 and 0.15 dpa, data are well fitted by a linear curve. Then, we observe a plateau, as for the 30 nm samples, but around 340 °C. It starts at the end of the superlinear damage accumulation regime, around 0.15 dpa (1 × 10¹⁴ ions/cm²) as we can see in Fig. 1. Above this value, the tendency between the defect accumulation and the damage dose becomes sublinear again, as for low implanted case.

In Fig. 4(b), we present the onset of the NiSi phase disappearance for 10 and 30 nm Ni. Between 0 and 0.15 dpa, the 10 nm Ni data follow a slightly decreasing linear relation while around 0.15 dpa, the temperature suddenly drops by about 400 °C and remains constant afterwards. The last points also correspond to the onset temperature of the NiSi₂ phase formation (~380 °C) according to time-resolved XRD. It is worth noting that between 0 and 0.15 dpa, no NiSi₂ diffraction peaks are visible, so it is not clear if the NiSi₂ phase is present or not. Thus, the decrease of the NiSi peak in low dpa cannot be attributed to the Ni consumption by NiSi₂ formation without uncertainty. For 30 nm Ni only a slight temperature decrease is observed with increasing damage dose, but no dramatic drop as in the 10 nm case. Experiments were made on samples implanted at 30 keV such that there is not enough a-Si (~60 nm) to supply the full conversion to NiSi₂ (~110 nm). The NiSi₂ phase formation starts at low temperature but stops as the a-Si is all consumed. In samples implanted at 60 keV (~100 nm of a-Si), the 30 nm Ni samples show a low temperature NiSi₂ phase formation (~450 °C) and a reduced NiSi phase duration.

Our results show clearly that there is a threshold fluence, around 1 × 10¹⁴ Si/cm² (0.15 dpa), above which the silicide formation is significantly modified, although full amorphization is not reached according to Fig. 1. The NiSi phase temperature range is shortened and the NiSi₂ phase appears at temperature below 450 °C. This last result agrees with past studies showing low temperature NiSi₂ formation on evaporated a-Si or ion-amorphized Si [7,17]. We attribute this change in the formation sequence to the presence of a fully amorphized Si layer, with no c-Si clusters left. Below this threshold, the behaviour of the NiSi phase formation seems to be dependent on the Ni thickness. For 30 nm, the onset temperature is almost constant while in the 10 nm Ni case, it follows linearly the quantity of damage.

We conclude that ion implantation cannot be used to reduce the onset temperature of the NiSi phase formation. On the contrary, the onset temperature increases with implanted Si. Ion implantation can be useful to influence the phase sequence and raise NiSi formation temperature or induce the formation of NiSi₂ in a NiSi layer at much lower temperature.

4. Conclusion

In this study we have investigated the influence of implantation damage in Si on the NiSi formation. It was found that above a threshold fluence of about 1 × 10¹⁴ Si/cm² (0.15 dpa) the silicidation is greatly modified. This fluence is near the end of the superlinear damage accumulation regime, but full amorphization has not been reached according to channelling measurements. The NiSi phase formation starts ~35 °C later and the NiSi₂ phase appears

~380 °C sooner for 10 nm and ~450 °C for 30 nm of Ni deposited with respect to the unimplanted case. It was also shown that for thinner Ni layer (10 nm), the NiSi formation onset temperature increases linearly with the implantation fluence.

Acknowledgements

The authors thank Peng Wei, Louis Godbout and Xavier Perraton for their support on the Tandetron accelerator, Roy Carruthers for sample preparations at IBM Yorktown and Jean Jordan-Sweet for support at the NSLS. The synchrotron XRD experiments were conducted under DOE Contract No. DE-AC02-76CH-0016. The project was partially supported by the FQRNT, the CRSNG and NanoQuébec.

References

- [1] L.J. Chen, *Silicide Technology for Integrated Circuits*, The IEE, London, 2004.
- [2] K.N. Tu, G. Ottaviani, U. Gösele, H. Föll, *J. Appl. Phys.* 54 (1983) 758.
- [3] D. Deduytsche, C. Detavernier, R.L. Van Meirhaeghe, C. Lavoie, *J. Appl. Phys.* 98 (2005) 033526.
- [4] C. Lavoie, C. Detavernier, C. Cabral Jr., F.M. d'Heurle, A.J. Kellock, J. Jordan-Sweet, J.M.E. Harper, *Microelectron. Eng.* 83 (2006) 2042.
- [5] D. Mangelinck, J.Y. Dai, J.S. Pan, S.K. Lahiri, *Appl. Phys. Lett.* 75 (1999) 1736.
- [6] S. Roorda, W.C. Sinke, J.M. Poate, D.C. Jacobson, S. Dierker, B.S. Dennis, D.J. Eaglesham, F. Spaepen, P. Fuoss, *Phys. Rev. B* 44 (1991) 3702.
- [7] Yu.N. Erokhin, F. Hong, S. Pramanick, G.A. Rozgonyi, *Appl. Phys. Lett.* 63 (1993) 3173.
- [8] C. Lavoie, C. Cabral Jr., L.A. Clevenger, J.M.E. Harper, J. Jordan-Sweet, K.L. Saenger, F. Doany, *Mat. Res. Soc. Symp. Proc.* 406 (1996) 163.
- [9] G.B. Stephenson, K.F. Ludwig, J. Jordan-Sweet, J. Mainville, Y.S. Wang, M. Sutton, *Rev. Sci. Instr.* 60 (1989) 1537.
- [10] A.B. Rodriguez Navarro, *Appl. Crystallogr.* 40 (2007) 631.
- [11] S. Gaudet, C. Coia, P. Desjardins, C. Lavoie, submitted for publication.
- [12] D.F. Wilson, O.B. Cavin, *Scripta Metall. Mater.* (Netherlands) 26 (1992) 85.
- [13] M. Mayer, SIMNRA Version 6.04, RESOLNRA Version 1.00.
- [14] C. Coia, *Microstructure and Growth Kinetics of Nickel Silicide Ultra-thin Films Synthesized by Solid-state Reactions*, PhD, École Polytechnique de Montréal, Montreal, Canada, 2009, 317 p.
- [15] L. Pelaz, L.A. Marqués, J. Barboïlla, *J. Appl. Phys.* 96 (2004) 5947.
- [16] F. Schiettekatte, S. Roorda, R. Poirier, M.O. Fortin, S. Chazal, R. Héliou, *Appl. Phys. Lett.* 77 (2000) 4322.
- [17] C.-D. Lien, M.-A. Nicolet, S.S. Lau, *Phys. Status Solidi (a)* 81 (1984) 123.